NON-LINEAR STATE ESTIMATOR FOR ADVANCED CONTROL OF AN ORC TEST RIG FOR GEOTHERMAL APPLICATION

Pili R.[1]*, Eyerer S.[1], Dawo F.[1], Wieland C.[1], Spliethoff H.[1]

[1]Technical University of Munich, Chair of Energy Systems,
Garching b. München, Germany
roberto.pili@tum.de

* Corresponding Author

ABSTRACT

Organic Rankine Cycle Systems (ORC) are able to convert efficiently low-temperature geothermal heat sources into mechanical and electrical power or combined heat and power. Especially when producing both heat and power, high operational flexibility is necessary to meet the heat demand and supply electricity in an efficient way. Advanced controllers, as linear quadratic integrators, can be used to guarantee the required flexibility of the ORC unit. Such advanced controllers rely on information on the system state, which is in general non-fully measurable. To reach this goal, state estimators are used and analyzed in this work. First, a dynamic model of an ORC test rig for geothermal application is developed and validated against experimental data, with relative mean squared error for the major variables lower than 1%. Subsequently, a non-linear state estimator for the ORC evaporator coupled with a screw expander is designed and tested on a benchmark case. The considered estimator is an Unscented Kalman Filter based on a finite volume model of the evaporator. The results show that the dynamic and observer model are in good agreement with the experimental data. The observer converges to the wall temperature of the heat exchanger with sufficient accuracy also when starting from a different initial state. The estimated states by the filter can be therefore integrated to advanced single- or multi-variable controllers to maximize the ORC net power output and revenues.

1. INTRODUCTION

Organic Rankine Cycle (ORC) power systems are increasingly contributing to reduce CO_2 emissions and fossil fuel consumption, as they can efficiently convert middle/low temperature heat sources from biomass, geothermal, waste heat and solar thermal applications. Geothermal ORC plants amount for 75% of the total installed ORC capacity worldwide and are the fastest growing field of application (Tartière and Astolfi, 2017). The ORC can produce electricity, mechanical power or combined heat and power. In the case of heat and power production, the plant is generally operated in order to meet primarily the heat demand (Eyerer *et al.*, 2019c) , which varies extensively during the year, with high demand in winter and low demand in summer (Wieland *et al.*, 2016). The portion of heat that is not supplied to the heating network (from 25% in winter up to 100% in summer) is fed to the power generation unit for production of electricity or mechanical power (Dawo *et al.*, 2019). For this reason, the ORC unit has to be highly flexible to cope with the large spread in operating conditions and maximize the power production.

The present work focuses on the development of a state estimator for advanced control of a geothermal plant with heat and power supply, in order to guarantee high flexibility and large power output for the ORC unit. Advanced controllers as Linear Quadratic Integral (LQI) controllers have the advantage of handling information on multiple variables, considering the couplings among them. This allows for a coordinated control of multiple manipulated variables. LQI controllers on ORC power systems have been proposed by Luong and Tsao (2014) for waste heat recovery from heavy-duty vehicles. Their work assumed a turbine as expander, and a moving boundary approach was considered for the evaporator. It was shown that the LQI outperforms the proportional-integral controller, however it is only able to track the pressure setpoint properly if three actuators are used instead of two. An LQI controller for waste

heat recovery with a turbine and moving boundary model of the evaporator is also discussed in Zhang *et al.* (2012). The results showed that satisfactory operation can be achieved, also against disturbances.

Both previous works do not specifically address the problem of state estimation. Different approaches are possible to reach this goal. The first approach consists of linearizing the system around one or more operating points and using a classical Luenberger observer (Corriou, 2004). This has the advantage of being a simple solution, but information on the non-linear behavior of the system is lost through the linearization process. To predict better the non-linear dynamics of the system, Extended Kalman Filters (EKF) and Unscented Kalman Filters (UKF) are proposed, whereas the second has shown to be more robust against uncertainties at the expense of larger computational effort (Corriou, 2004). A UKF for waste heat recovery with ORC using a turbo-expander from an oil platform was discussed by Pierobon *et al.* (2014). It was shown that the UKF is robust with respect to process noise, measurement disturbances and initial conditions. In this article, an UKF to estimate the state of the evaporator of an ORC test rig based on a screw expander for geothermal application is developed. Section 2 describes the ORC test rig and its major components before the development and validation of the dynamic model are presented in Section 3. Section 4 discusses the development of the non-linear observer and the results, followed by the conclusions.

2. ORC TEST RIG AND CURRENT CONTROL STRATEGY

The ORC test rig is fully instrumented, with a temperature and pressure sensor up- and downstream of each major component and a magnetic-inductive flowmeter in the heat source loop and a Coriolis flowmeter in the ORC. The utilized working fluid was R1233zd(E), which is a low-GWP alternative to R245fa (Eyerer *et al.*, 2019b). Fig. 1 shows a simplified P&I diagram of the test rig and the control loops. A hot water loop serves as heat source for the ORC. It consists of an electrical resistance heater with 200 kW electrical power, which is controlled by pulse width modulation in order to adjust the heat source temperature at the evaporator inlet. The mass flow rate in the heat source loop is controlled by varying the rotational speed of a centrifugal pump. On the working fluid side, the fluid leaves the evaporator superheated and enters the expander. The expansion machine is an open drive twin-screw volumetric compressor from Bitzer (OSN5361-K), which is operated in reverse mode. The machine has a swept volume of 0.6781 l on the low-pressure side and a volume ratio of 3.1. By varying the rotational speed of the expander, the pressure of the incoming vapor can be controlled. The machine is directly coupled with the generator shaft. The rotational speed of the expander/generator shaft is controlled via

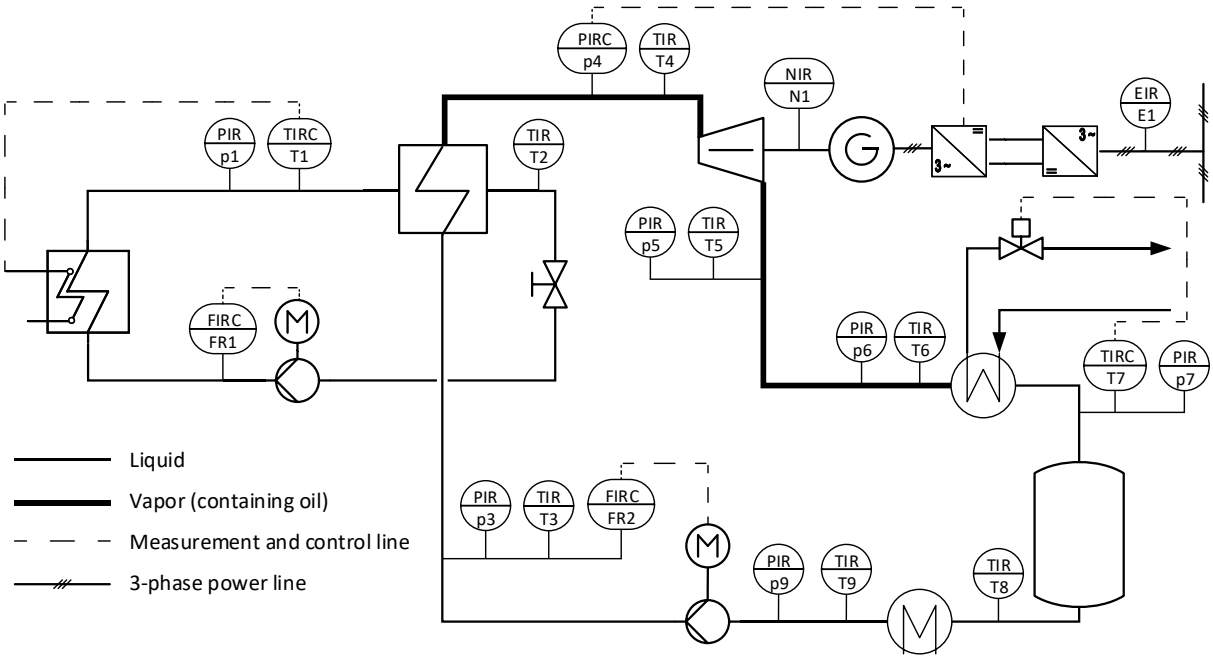

Figure 1: Simplified P&I diagram of the ORC test rig.

a frequency converter. The produced electricity is measured and fed into the campus grid. After the expander, the low pressure vapor enters the condenser, where it is desuperheated and fully condensed. The cooling water is taken from a local grid. A control valve in the cooling water line defines the mass flow rate of cooling water and is utilized to control the condensation temperature. Subsequently, the condensate flows into a 30 l buffer tank and is then slightly subcooled in the subcooler. The subcooling is done to prevent cavitation in the following piston diaphragm pump, which forwards the fluid to the high pressure part of the ORC. The rotational speed of the pump is controlled to adjust the mass flow rate of the working fluid and thus the superheating at the expander inlet. The pressurized working fluid then enters the evaporator and gets preheated, evaporated and superheated to close the cycle. All heat exchangers are brazed plate heat exchangers from Alfa Laval. Table 1 summarizes all the instrumentation and measuring ranges as well as the accuracy of each sensor. For a more detailed description of the test rig, reference is made to Eyerer *et al.* (2019a).

Table 1: Measuring range and accuracy of the relevant sensors

Measured parameter	Measurement principle	Measuring range	Accuracy of measurement	Sensors	Output signal
Pressure	Strain gauge	0 - 16 bar 0 - 40 bar 0 - 60 bar	±0.16 bar ±0.40 bar ±0.60 bar	p5-p9 p4 p3	4-20 mA
Temperature	PT100	-100 - 400 °C 0 - 150 °C	±(0.002·MV+0.15 °C) ±(0.0017·MV+0.1 °C)	T3 All other	resistance
Total mass flow rate	Coriolis sensor	0 - 1.5 kg/s	±(0.0015·MV+ 0.7502 kg/s)	FR2	4-20 mA
El. gross power output	El. power meter	0 - 40 kW	±0.01·MV	E1	digital

3. DYNAMIC MODEL OF THE ORC TEST RIG AND VALIDATION

A dynamic model of the ORC test rig is developed in Dymola (Dassault Systemes, 2018), by using the commercial TIL library (TLK-Thermo GmbH, 2018). The thermodynamic properties of R1233zd(E) are retrieved from REFPROP (Lemmon *et al.*, 2017). The heat exchangers are modelled as finite volume heat exchangers with 15 cells, based on the authors' experience and good agreement with experimental data. The main geometric parameters are summarized in Table 2, whereas the heat transfer and pressure drop correlations are listed in Table 3.

Table 2: Geometric features of test rig heat exchangers

Heat exchanger	Plate width, mm	Plate length, mm	Number of plates, -	Chevron angle*, °	Plate distance*, mm
Evaporator	191	519	52	75	1.60
Condenser	191	519	170	75	1.60
Subcooler	113	466	60	65	1.95

*Estimated from measurement data.

For the subcooler, a better agreement has been found by multiplying the heat transfer coefficient based on the Martin (2010) correlation by a factor equal to 2. The pressure drops for the heat and cold sources have been neglected for simplicity. The expander is a volumetric machine, whose model is depicted in Fig. 2 and based on Lemort *et al*. (2009). The fluid enters the machine at high pressure from the left and proceeds to the right in the figure. A pressure drop represented by a throttle valve can occur at the suction port before reaching the suction inner volume. Here the fluid is slightly heated up by half of the friction losses occurring at the bearings. A portion of the fluid undergoes the expansion inside the machine contributing to the torque at the machine shaft. Depending on the pressure at the end of the expansion and the pressure at the discharge volume, an isentropic, under- or overexpansion can take place. Due to internal leakages, a portion of the flow moves directly from the suction to the discharge volume by reducing its pressure isenthalpically. At the discharge, half of the friction losses at the

Table 3: Heat transfer and pressure drop correlation for heat exchangers

Component	Fluid		Heat transfer and pressure drop correlation	
	Hot side	Cold side	Hot side	Cold side
Evaporator	Hot water	Working fluid	Martin (2010), (only heat)	Single phase: Martin (2010); Two-phase: Amalfi *et al.* (2016)
Condenser	Working fluid	Cooling water	Single phase: Martin (2010); Two-phase: Yan *et al.* (1999)	Martin (2010), (only heat)
Subcooler	Working fluid	Cooling water	2 x Martin (2010)	Martin (2010), (only heat)

bearings is transferred to the fluid, which also exchanges heat to the surroundings. Before the fluid leaves the expander, a pressure drop can then occur at the discharge port, modelled again by means of a throttle valve. Several parameters, i.e., the suction and discharge throttle cross-sectional areas, the leakage cross-sectional area as well as the heat loss coefficient UA have been determined by fitting from experimental data, assuming an ambient temperature of 25°C.

The pressure drop in pipes has been modelled according to the following equation:

$$\Delta p = c_0 \, \Delta p_{nom} \left(\frac{\dot{m}}{\dot{m}_{nom}} \right)^{c_1} \tag{1}$$

where c_0 and c_1 are listed in Table 4, together with their nominal values. The pressure drop between the pump and the evaporator has been divided into two parts for better agreement with the experimental data. The pressure drop in the connecting pipes between the condenser, the condensate receiver and the subcooler are neglected. For the generator and inverter, a design efficiency of 89.8% and 96.9% is assumed. Mechanical losses between the expander and the generator amounted 9.5% at nominal point. The part-load behavior has been predicted using the part-load efficiency functions for electric motor (being the generator a reversed induction motor) and inverter defined in Pili *et al.* (2019).

To validate the ORC dynamic model, experiments have been carried out on test rig varying stepwise the manipulated variables (rotational speed of the ORC pump, rotational speed of the expander and opening of the cooling water valve at the condenser). The data have been collected with 1-second time step. The time behavior of the three manipulated variables is shown in Fig. 3, together with the response of the system. It is clear that the rotational speed of the pump directly affects the mass flow rate of working fluid, whereas the rotational speed of the expander has a direct impact on the evaporator pressure. The resulting conditions in the evaporator affect then the outlet temperature of the working fluid. The condensing pressure is in turn directly influenced by the mass flow rate of cooling water, which is controlled by a valve in the cooling water loop.

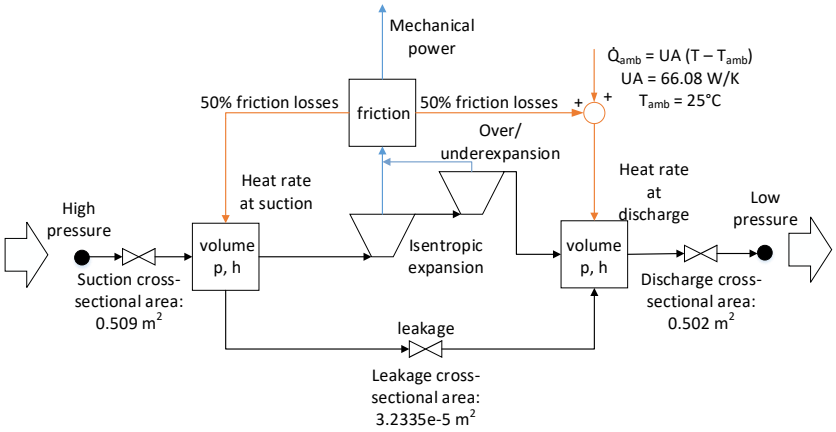

Figure 2: Expander model with fitting parameters.

Table 4: Pressure drop in pipes

Pipe	$\dot{m}_{nom}$, kg/s	Δp_{nom}, bar	c_0, -	c_1, -
Pump – evaporator (part 1)	0.6898	0.4184	0.9929	1.9364
Pump – evaporator (part 2)	0.6898	0.0395	1.1300	0.8861
Evaporator - expander	0.6898	1.4370	0.9908	1.5907
Expander - condenser	0.6898	0.5800	1.1899	1.3740

The test case is simulated in Dymola by setting the manipulated variables as measured. The simulation results are shown with dashed line in Fig. 3. It can be seen that the dynamic model predicts the system response with good accuracy, with slight over-prediction of the pressure at the evaporator outlet p4 at higher values and under-prediction of the working fluid outlet temperature T4 at low values. The expander outlet temperature T5 follows the under-prediction of T4 and shows slight over-prediction at the positive step changes. The relative mean squared error for major variables is illustrated in Table 5 and is for all quantities < 1%.

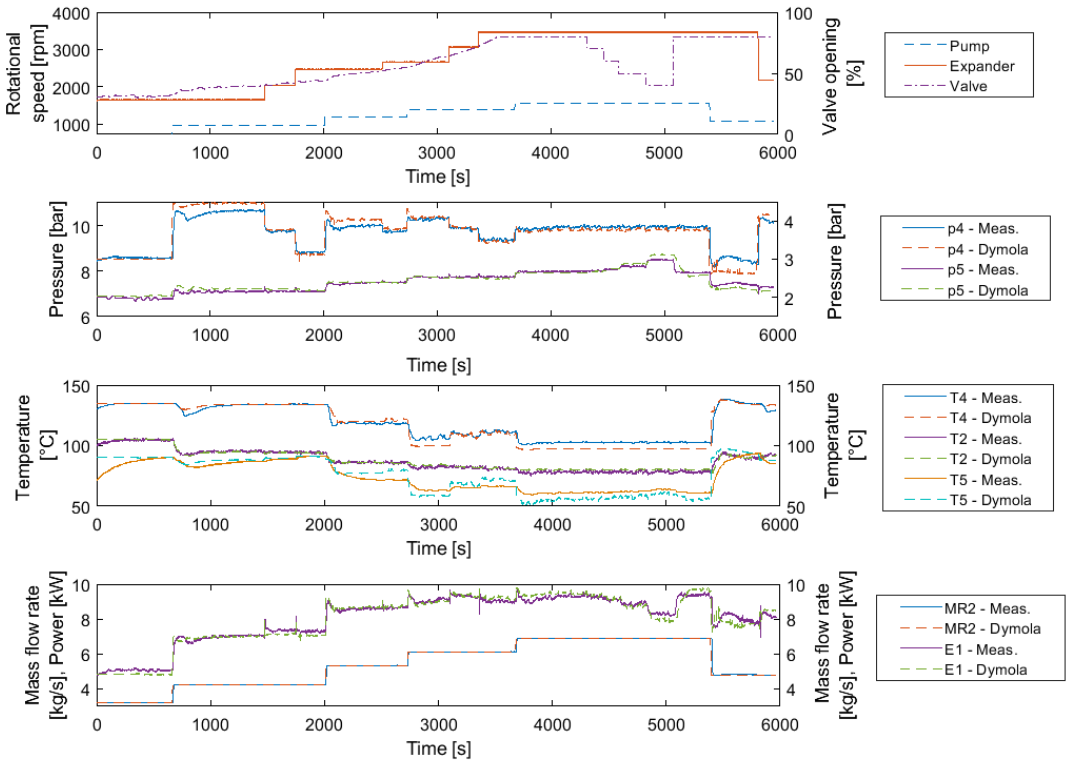

Figure 3: Comparison of experimental data ('Meas.') and simulation in Dymola ('Dymola').

To illustrate the validity of the expander and ORC model, 17 steady-state points have been determined from the experiment of Fig. 3 by averaging the results after the dynamic transients. Fig. 4 depicts a comparison of the ORC gross electrical efficiency $\eta_{el,ORC,gross}$ and the expander-to-electrical isentropic efficiency $\eta_{exp-to-el,is,gross}$, defined as:

$$\eta_{el,ORC,gross} = \frac{P_{el,gross}}{\dot{Q}_{eva,ORC}} \tag{2}$$

$$\eta_{exp-to-el,is,gross} = \frac{P_{el,gross}}{\dot{m}_{wf}\left(h_{eva,out} - h_{exp,out,is}\right)} \tag{3}$$

where $P_{el,gross}$ is the electrical power from the inverter, $\dot{Q}_{eva,ORC}$ the heat rate at the evaporator transferred to the ORC, $\dot{m}_{wf}$ the mass flow rate of working fluid, $h_{eva,out}$ the specific enthalpy at evaporator outlet and $h_{exp,out,is}$ the specific enthalpy at the expander outlet in the case of isentropic expansion. It can be seen that the deviation between the simulation in Dymola and measurements is within ± 5 %.

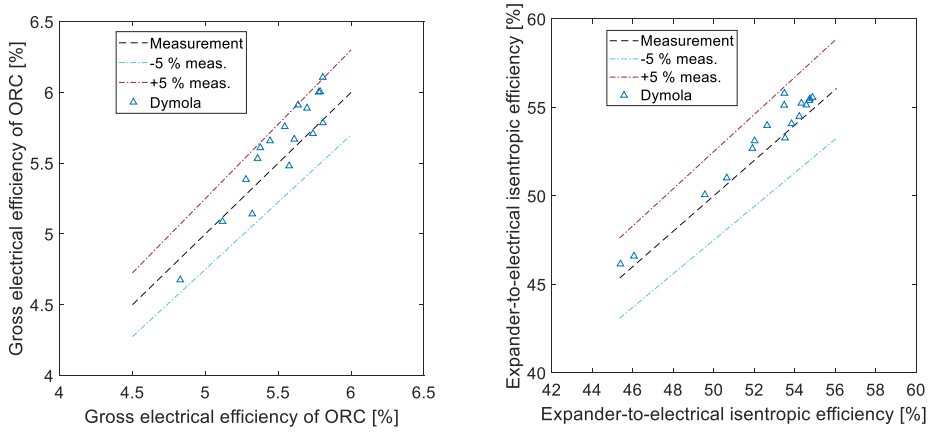

Figure 4: Comparison of ORC electrical and expander-to-electrical isentropic efficiencies between experimental data ('Measurement') and simulation in Dymola ('Dymola').

4. NON-LINEAR ESTIMATION OF EVAPORATOR STATE

A non-linear discrete-time observer is presented in the following to estimate the state of the evaporator. This component is crucial for the system performance, since it determines the conditions at the expander inlet and therefore the available thermal power for the expander. To control the ORC unit more efficiently, a knowledge of the evaporator states is therefore required. The evaporator is modelled in Simulink® (MathWorks, 2018) as discretized finite volumes where energy and mass balances are solved. To reduce the computational effort, a lower number of cells (10) than in Dymola is chosen and the pressure drop is neglected inside the evaporator and included with a fitting function after the

Table 5: Relative mean squared error between dynamic model and experimental data

Quantity	Point in Fig. 1	RMSE, %
Pressure of working fluid at evaporator outlet	p4	0.08
Temperature of working fluid at evaporator outlet	T4	0.01
Temperature of hot water at evaporator outlet	T2	0.00
Temperature of working fluid at expander outlet	T5	0.03
Pressure of working fluid at expander outlet	p5	0.10
Electric power at inverter outlet	E1	0.11

evaporator. The evaporator states are the cell wall temperatures (10 states), the cell specific enthalpies of the working fluid (10 states) and heat source (10 states) and the cell pressure for the working fluid (1 state, same for all cells). The cell heat transfer coefficients for the working fluid (10 states) is also considered as a state α_{st}, since a filter of the form:

$$\frac{d\alpha_{st}}{dt} = \frac{\alpha - \alpha_{st}}{T_\alpha} \tag{4}$$

is used to avoid discontinuities when the cell heat transfer coefficient α sharply changes because of phase change. The time constant T_α is set to 3 s. For the same reason, a filter with small time constant at 0.1 s is also considered for the time derivative of pressure for the working fluid. The heat source is assumed as incompressible fluid at constant pressure. This results in a total of 42 state variables for the estimator. The fluid properties are retrieved by means of interpolation of look-up tables based on REFPROP for both fluids (Lemmon *et al.*, 2017). The heat transfer coefficients have been simplified from fitting of the results of the previous simulation as follows:

$$\alpha = \alpha_{nom} \left(\frac{\dot{m}}{\dot{m}_{nom}} \right)^{\gamma} \tag{5}$$

where $\gamma = 0.66$ for both fluids and all phases. A steady-state model of the twin-screw expander has been modelled based on Fig. 2 as well to predict the pressure development if changes in working fluid mass flow rate and expander rotational speed occur.

The Unscented Kalman Filter (UKF) has proven being able to capture better the dynamics of a non-linear system with respect to the Extended Kalman Filter, and it is hence chosen in the following. A description of the steps applied to estimate the system state can be found in Pierobon *et al.* (2014). The UKF is based on two tuning parameters: $0 \leq \alpha \leq 1$ and $\kappa \geq 0$. After some preliminary tests, $\alpha = 0.1$ and $\kappa = 0$ are chosen. A third weight parameter is β, which is equal to 2 for Gaussian distribution. The UKF sample time is set to 0.5 s, whereas the evolution of the state function is determined with 75 intermediate steps to keep the filter stable and robust against initial values and fast state changes. The observer estimates the state from a limited number of measurable variables, which in this case are the outlet temperatures of working fluid (T4) and hot water (T2), as well as the pressure in front of the expander (p4 minus pressure drop between evaporator and expander, p4'). Since the dynamics of the heat exchanger is mainly determined by the temperature of the metallic wall, this is analyzed in the following and will be compared with the validated dynamic model in Dymola.

The step change in expander rotational speed between t = 1905 s and t = 2400 s of Fig. 3, in which the speed varies from 2470 rpm to 2663 rpm, has been considered to prove the UKF concept. The initial outlet temperature of the working fluid T4 is approximately 3 K lower than the measured value. It can be seen in Fig. 5 that the observer converges in less than 50 s towards the measured T4 and estimates it with high accuracy. In this simulation section, T4 simulated with Dymola is slightly higher than the measurement. The main reason for this is the larger overshoot in pressure p4 after the step change, which results in a higher evaporation temperature and then higher T4. The wall temperatures of the evaporator predicted by the UKF and Dymola, important for the dynamics and the space-state controller, are also shown at inlet ('1'), middle ('M') and outlet ('N') of the heat exchanger. The prediction of the pressures p4 and p4' is also in good agreement with the measurements. The simulated pressures are affected by peaks, because of the discontinuity in density when the phase in a cell changes (Pili *et al.*, 2019). This is an intrinsic problem of finite volume heat exchangers with phase change, and it is more significant for the UKF than the simulation in Dymola, since the number of cells is lower (10 against 15 cells). The peaks in pressure would be reduced if the number of cells would be increased, but it would cost higher computational effort. However, given the good accuracy of the state prediction, the observer can be used with sufficient confidence to estimate the state of the evaporator and predict the dynamics for given heat source inlet conditions, rotational speed of the pump and of the expander.

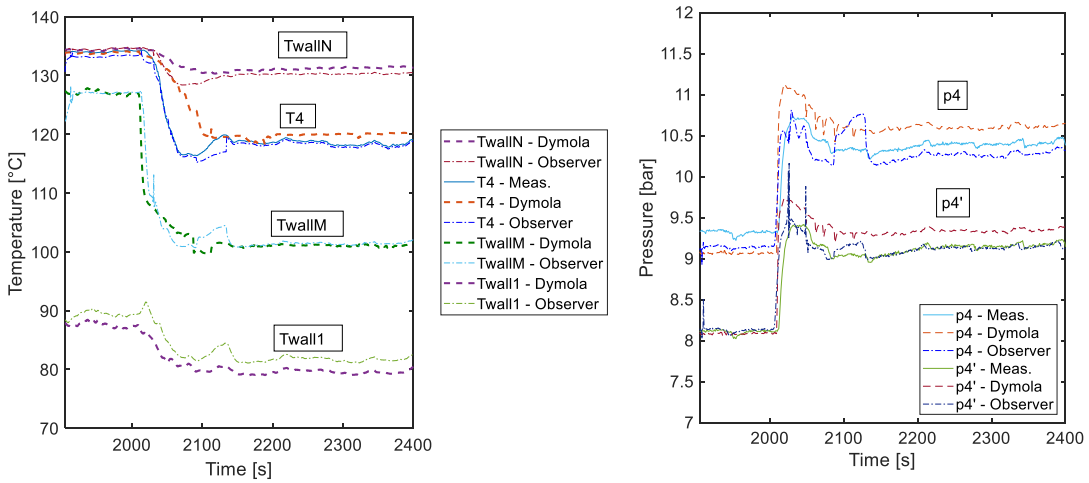

Figure 5: Observer performance with respect to experimental data and dynamic model in Dymola.

5. CONCLUSIONS

To guarantee flexibility of geothermal plants with heat and power production, multivariable advanced controllers as linear quadratic integrators can be used. These controllers require the estimation of the system state, which is in general non-fully measurable. In this work, a dynamic model of an ORC test rig with twin-screw expander was developed and validated against experimental data, with relative mean squared error for the major variables lower than 1%. An Unscented Kalman Filter was used as state estimator for the ORC evaporator and expander, and its performance has been compared to the experimental data and dynamic model. Both the dynamic model and state estimator showed high agreement with the experimental data. As part of future work, the observer will be integrated in an advanced controller and the control performance of the ORC unit will be tested under changes in electric load and heat source both via simulations and experiments on the test rig.

NOMENCLATURE

c	fitting coefficient	(-)
Δp	pressure drop	(bar)
E	electric power	(W)
h	specific enthalpy	(J/kg)
MR	mass flow rate	(kg/s)
$\dot{m}$	mass flow rate	(kg/s)
P	power	(W)
p	pressure	(bar)
$\dot{Q}$	heat rate	(W)
RMSE	root mean squared error	(-)
T	time constant	(s)
t	time	(s)
UA	thermal capacity	(W/K)
α	heat transfer coefficient/ coefficient for UKF	(W/m^2K, -)
β	coefficient for UKF	(-)
γ	fitting exponent	(-)
η	efficiency	(-)
κ	coefficient for UKF	(-)

Subscript

eva	evaporator
is	isentropic
nom	nominal
out	outlet
st	state
p	participants
wf	working fluid

Abbreviations

EKF	Extended Kalman Filter
LQI	Linear Quadratic Integral Controller
ORC	Organic Rankine Cycle
UKF	Unscented Kalman Filter

REFERENCES

Amalfi, R. L., Vakili-Farahani, F., Thome, J. R., 2016, Flow boiling and frictional pressure gradients in plate heat exchangers. Part 2. Comparison of literature methods to database and new prediction methods, *Int. J. Refrig.*, vol. 61: p. 185–203.

Corriou, J.-P., 2004, *Process Control. Theory and Applications*, Springer London, London, 867.

Dassault Systemes, 2019, *Dymola - Dynamic Modeling Laboratory*, 64-bit, FD2019.

Dawo, F., Wieland, C., Spliethoff, H., 2019, Kalina power plant part load modeling. Comparison of different approaches to model part load behavior and validation on real operating data, *Energy*, vol. 174: p. 625–637.

Eyerer, S., Dawo, F., Pili R., Niederdränk, A., Windhager, R., Wieland, C., Spliethoff H., 2019a, Advanced Injection Cooling Concept for Organic Rankine Cycles. *32nd International Conference on Efficiency, Cost, Optimization, Simulation and Environmental Impact of Energy Systems.*

Eyerer, S., Dawo, F., Kaindl, J., Wieland, C., Spliethoff, H., 2019b, Experimental investigation of modern ORC working fluids R1224yd(Z) and R1233zd(E) as replacements for R245fa, *Appl. Energ.*, vol. 240: p. 946–963.

Eyerer, S., Schifflechner, C., Hofbauer, S., Bauer, W., Wieland, C., Spliethoff, H., 2019c, Combined heat and power form hydrothermal geothermal resources in Germany: An assessment of the potential, *Renew Sust. Energ. Rev*. *(Submitted)*.

Lemmon, E. W., Bell, I. H., Huber, M. L., McLinden, M. O., 2017, *NIST Standard Reference Database 23: Reference Fluid Thermodynamic and Transport Properties-REFPROP 9.1*, Gaithersburg: National Institute of Standards and Technology, Standard Reference Data Program.

Lemort, V., Quoilin, S., Cuevas, C., Lebrun, J., 2009, Testing and modeling a scroll expander integrated into an Organic Rankine Cycle, *Appl. Therm. Eng.*, vol. 29, no. 14-15: p. 3094–3102.

Luong, D., Tsao, T.-C., 2014, Linear Quadratic Integral control of an Organic Rankine Cycle for waste heat recovery in heavy-duty diesel powertrain, *American Control Conference (ACC)*, American Automatic Control Council: p. 3147–3152.

Martin, H., 2010, Pressure Drop and Heat Transfer in Plate Heat Exchangers, Section N6 in *VDI Heat Atlas*, 2. ed. Heidelberg: Springer, 1608.

MathWorks, 2019, *MATLAB®/Simulink®*, 2019a.

Pierobon, L., Schlanbusch, R., Kandepu, R., Haglind, F., 2014, Application of Unscented Kalman Filter for Condition Monitoring of an Organic Rankine Cycle Turbogenerator, *Proceedings of the Annual Conference of the Prognostics and Health Management Society*, Prognostics and Health Management Society.

Pili, R., Romagnoli, A., Jimenez-Arreola, M., Spliethoff, H., Wieland, C., 2019: Simulation of Organic Rankine Cycle – Quasi-steady state vs dynamic approach for optimal economic performance, *Energy*, vol. 167: p. 619–640.

Tartière, T., Astolfi, M., 2017, A World Overview of the Organic Rankine Cycle Market, *Energy Proced.*, vol. 129: p. 2–9.

TLK-Thermo GmbH, 2018, *TIL Library 3.5.0*.

Wieland, C., Meinel, D., Eyerer, S., Spliethoff, H., 2016, Innovative CHP concept for ORC and its benefit compared to conventional concepts, *Appl. Energ.*, vol. 183: p. 478–490.

Yan, Y.-Y., Lio, H.-C., Lin, T. F., 1999: Condensation heat transfer and pressure drop of refrigerant R-134a in a plate heat exchanger, *Int. J. Heat Mass Tran.*, vol. 42, no. 6: p. 993–1006.

Zhang, J., Zhang, W., Hou, G., Fang, F., 2012, Dynamic modeling and multivariable control of organic Rankine cycles in waste heat utilizing processes, *Computers & Mathematics with Applications*, vol. 64, no. 5: p. 908–921.

ACKNOWLEDGEMENT

The work has been developed as part of project Geothermal-Alliance Bavaria funded by the Bavarian State Ministry of Education, Science and Arts, which is here gratefully acknowledged.